PSI-PR-97-31
KA-TP-16-1997
hep-ph/yymmnnn

Radiative Corrections to $W^+W^- \to W^+W^-$ in the Electroweak Standard Model

A. Denner

Paul-Scherrer-Institut, Würenlingen und Villigen
CH-5232 Villigen PSI, Switzerland

T. Hahn

Institut für Theoretische Physik, Universität Karlsruhe
D-76128 Karlsruhe, Germany

Abstract:

The cross-section for $W^+W^- \to W^+W^-$ with arbitrarily polarized W bosons is calculated within the Electroweak Standard Model including the complete virtual and soft-photonic $\mathcal{O}(\alpha)$ corrections. We show the numerical importance of the radiative corrections for the dominating polarized cross-sections and for the unpolarized cross-section. The numerical accuracy of the equivalence theorem is investigated in $\mathcal{O}(\alpha)$ by comparing the cross-section for purely longitudinal W bosons obtained from the equivalence theorem and from the direct calculation. We point out that the instability of the W boson, which is inherent in the one-loop corrections, prevents a consistent calculation of radiative corrections to the scattering of on-real-mass-shell longitudinal W bosons beyond $\mathcal{O}(\alpha)$.

November 1997

1 Introduction

Gauge-boson scattering provides a direct way to probe both the non-abelian and scalar sector of the Electroweak Standard Model (SM). Since in lowest order all gauge-boson scattering amplitudes involve only interactions between gauge and scalar bosons, the corresponding cross-sections depend very sensitively on the non-abelian and scalar sector of the underlying theory. This sensitivity is even enhanced for high-energetic, longitudinally polarized, massive gauge bosons owing to the presence of gauge cancellations. For these reasons, gauge-boson scattering has found continuous interest in the literature [1–4] since the early years of spontaneously broken gauge theories. The sensitivity of gauge-boson scattering to the non-abelian gauge couplings has been investigated, for instance, in Ref. [5].

Gauge-boson scattering can be studied in principle at all high-energy colliders, such as pp colliders like the LHC [6], e^+e^- colliders like the proposed NLC [7], or $\mu^+\mu^-$ colliders [8]. These reactions naturally appear as subprocesses, e.g. as final-state interactions in hadron or lepton collisions. At high energies ($E \gg M_W$) the incoming particles radiate plenty of gauge bosons. Similar to the well-known Weizsäcker–Williams approximation for photonic reactions also massive vector-boson scattering at high energies can be approximated by convoluting the vector-boson cross-section with the corresponding flux of vector bosons. This approximation is known as the *equivalent vector-boson method* (see e.g. Ref. [9] and references therein).

Gauge-boson scattering reactions have been studied at tree level in Ref. [1]. So far, only the leading radiative corrections in the limit of high energies and large Higgs-boson masses ($E, M_H \gg M_W$) have been calculated [2–4]. In most of these calculations the scattering of only longitudinal gauge bosons was considered, and the Goldstone-boson equivalence theorem [10] was used. A complete $\mathcal{O}(\alpha)$ calculation was available only for the process $\gamma\gamma \to W^+W^-$ [11,12].

In a recent paper [13] the complete one-loop electroweak radiative corrections to the simplest massive gauge-boson scattering process, $ZZ \to ZZ$, have been discussed. By means of this example many characteristic features of massive gauge-boson scattering processes could be studied at the one-loop level, such as the treatment of the Higgs-boson resonance and the gauge cancellations, which are quantitatively expressed by the Goldstone-boson equivalence theorem.

In this paper we perform a similar study of elastic W^+W^- scattering, which is one of the dominating gauge-boson scattering processes at all energies. Because the W bosons are charged, real bremsstrahlung corrections are required that lead to additional complications. Since we are mainly interested in the weak corrections, we include these corrections only in the soft-photon limit and omit the radiation of hard photons that depends on the experimental situation. Moreover, we restrict our discussion to the case of a relatively light Higgs boson so that no Higgs resonance occurs. Such a light Higgs boson is favoured by precision experiments [14]. Furthermore, the treatment of the Higgs resonance requires to include higher-order corrections. But as we show in this paper, the calculation of corrections of order α^2 or higher for the scattering of on-real-mass-shell longitudinal W bosons becomes inconsistent owing to the finite width of the W bosons, which enters unavoidably via loop diagrams.

This paper is organized as follows: After some preliminary remarks about kinematics, conventions, and discrete symmetries in Section 2, we discuss the lowest-order cross-sections in Section 3. In Section 4 we describe the explicit calculation and the structure of the $\mathcal{O}(\alpha)$ corrections. Numerical results are presented in Section 5. Section 6 is devoted to a discussion of problems that occur in the calculation of the radiative corrections to $\mathrm{W^+W^-} \to \mathrm{W^+W^-}$ beyond $\mathcal{O}(\alpha)$. Section 7 contains our conclusions.

2 Kinematics, notation, and discrete symmetries

We consider the reaction

$$\mathrm{W}^+(k_1,\lambda_1) + \mathrm{W}^-(k_2,\lambda_2) \to \mathrm{W}^+(k_3,\lambda_3) + \mathrm{W}^-(k_4,\lambda_4)\,, \tag{1}$$

where k_i and λ_i represent the momenta and helicities of the W bosons, respectively. In the following, the indices L, T, and U denote longitudinal ($\lambda_i = 0$), transverse ($\lambda_i = \pm$) and unpolarized W bosons, respectively, and definite polarization combinations are labelled by a sequence of four letters, e.g. LTLT stands for $\mathrm{W_L^+W_T^-} \to \mathrm{W_L^+W_T^-}$.

The incoming particles travel along the z axis and are scattered into the x–z plane. In the centre-of-mass system (CMS) the momenta and polarization vectors $\varepsilon_i(\lambda_i)$ explicitly read

$$\begin{aligned}
k_1^\mu &= (E,\,0,\,0,\,-p)\,, & k_3^\mu &= (E,\,-p\sin\theta,\,0,\,-p\cos\theta)\,,\\
\varepsilon_1^\mu(0) &= (-p,\,0,\,0,\,E)\,/M_\mathrm{W}, & \varepsilon_3^{\mu,*}(0) &= (p,\,-E\sin\theta,\,0,\,-E\cos\theta)\,/M_\mathrm{W},\\
\varepsilon_1^\mu(\pm) &= (0,\,-1,\,\pm\mathrm{i},\,0)\,/\sqrt{2}\,, & \varepsilon_3^{\mu,*}(\pm) &= (0,\,-\cos\theta,\,\mp\mathrm{i},\,\sin\theta)\,/\sqrt{2}\,,\\
k_2^\mu &= (E,\,0,\,0,\,p)\,, & k_4^\mu &= (E,\,p\sin\theta,\,0,\,p\cos\theta)\,,\\
\varepsilon_2^\mu(0) &= (-p,\,0,\,0,\,-E)\,/M_\mathrm{W}, & \varepsilon_4^{\mu,*}(0) &= (p,\,E\sin\theta,\,0,\,E\cos\theta)\,/M_\mathrm{W},\\
\varepsilon_2^\mu(\pm) &= (0,\,1,\,\pm\mathrm{i},\,0)\,/\sqrt{2}\,, & \varepsilon_4^{\mu,*}(\pm) &= (0,\,\cos\theta,\,\mp\mathrm{i},\,-\sin\theta)\,/\sqrt{2}
\end{aligned} \tag{2}$$

in terms of the energy E of the W bosons, their momentum $p = \sqrt{E^2 - M_\mathrm{W}^2}$, and the scattering angle θ. The Mandelstam variables are defined as

$$\begin{aligned}
s &= (k_1+k_2)^2 = 4E^2\,,\\
t &= (k_1-k_3)^2 = -4p^2\sin^2\theta/2\,,\\
u &= (k_1-k_4)^2 = -4p^2\cos^2\theta/2\,.
\end{aligned} \tag{3}$$

The polarized differential cross-section is obtained from the invariant matrix element $\mathcal{M}$ as

$$\left(\frac{\mathrm{d}\sigma}{\mathrm{d}\Omega}\right)_{\lambda_1\lambda_2\lambda_3\lambda_4} = \frac{1}{64\pi^2 s}\left|\mathcal{M}_{\lambda_1\lambda_2\lambda_3\lambda_4}\right|^2, \tag{4}$$

and the unpolarized cross-section results from averaging over the polarizations of the incoming and summing over the polarizations of the outgoing particles,

$$\left(\frac{\mathrm{d}\sigma}{\mathrm{d}\Omega}\right)_\mathrm{unpol} = \frac{1}{9}\sum_{\lambda_1,\lambda_2=-1}^{1}\;\sum_{\lambda_3,\lambda_4=-1}^{1}\left(\frac{\mathrm{d}\sigma}{\mathrm{d}\Omega}\right)_{\lambda_1\lambda_2\lambda_3\lambda_4}. \tag{5}$$

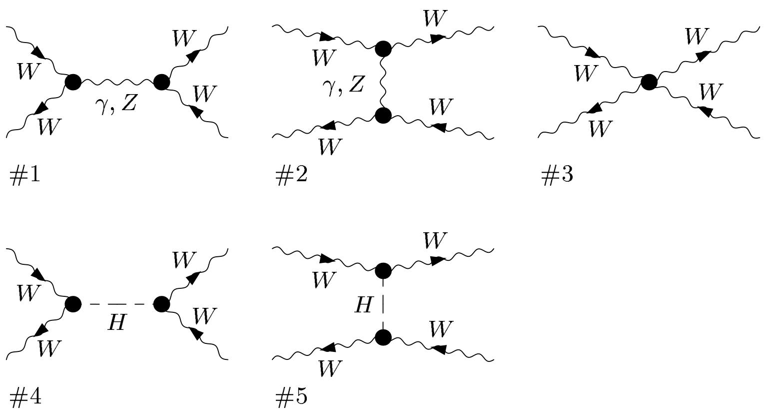

Figure 1: The lowest-order diagrams contributing to $W^+W^- \to W^+W^-$.

More generally, the correct average is obtained by multiplying with 1/3 for each unpolarized W boson and by 1/2 for each transverse W boson in the initial state.

The integrated cross-section is defined by

$$\sigma = \int_{0^\circ}^{360^\circ} \mathrm{d}\varphi \int_{\theta_{\mathrm{cut}}}^{180^\circ - \theta_{\mathrm{cut}}} \mathrm{d}\theta \, \sin\theta \, \frac{\mathrm{d}\sigma}{\mathrm{d}\Omega}, \tag{6}$$

where θ_{cut} denotes an angular cut which is set to 10° in the numerical calculations.

Discrete symmetries relate different helicity amplitudes. CPT symmetry implies

$$\mathcal{M}_{\lambda_1\lambda_2\lambda_3\lambda_4} = \mathcal{M}_{\lambda_3\lambda_4\lambda_1\lambda_2}\,. \tag{7}$$

Since we neglect quark mixing, also CP is conserved and as a consequence, the helicity amplitudes are related as follows

$$\mathcal{M}_{\lambda_1\lambda_2\lambda_3\lambda_4} = \mathcal{M}_{-\lambda_2-\lambda_1-\lambda_4-\lambda_3}\,. \tag{8}$$

These symmetries reduce the number of independent polarized amplitudes from 81 to 27.

3 Lowest-order cross-sections

3.1 General properties

In lowest order, seven Feynman diagrams exist for $W^+W^- \to W^+W^-$ as shown in Fig. 1. Owing to charge conservation there are no u-channel diagrams, and therefore the cross-section is expected to have a forward–backward asymmetry. The resulting tree-level amplitude reads

$$\begin{aligned}\mathcal{M}_{\mathrm{Born}} = & -e^2\left(\frac{1}{s} + \frac{c_{\mathrm{W}}^2}{s_{\mathrm{W}}^2}\frac{1}{s-M_{\mathrm{Z}}^2}\right)\mathcal{M}_1 - e^2\left(\frac{1}{t} + \frac{c_{\mathrm{W}}^2}{s_{\mathrm{W}}^2}\frac{1}{t-M_{\mathrm{Z}}^2}\right)\mathcal{M}_2 \\ & -\frac{e^2}{s_{\mathrm{W}}^2}\mathcal{M}_3 - \frac{e^2 M_{\mathrm{W}}^2}{s_{\mathrm{W}}^2}\frac{1}{s-M_{\mathrm{H}}^2}\mathcal{M}_4 - \frac{e^2 M_{\mathrm{W}}^2}{s_{\mathrm{W}}^2}\frac{1}{t-M_{\mathrm{H}}^2}\mathcal{M}_5\,.\end{aligned} \tag{9}$$

The matrix elements $\mathcal{M}_1$–$\mathcal{M}_5$ correspond to the diagrams #1– #5 in Fig. 1, respectively, and contain the complete kinematical information and polarization dependence,

$$\begin{aligned}
\mathcal{M}_1 = {} & (\varepsilon_1\cdot\varepsilon_2)(\varepsilon_3^*\cdot\varepsilon_4^*)(t-u) \\
& + 4\Big\{(\varepsilon_1\cdot\varepsilon_2)\big[(\varepsilon_3^*\cdot k_4)(\varepsilon_4^*\cdot k_2)-(\varepsilon_3^*\cdot k_2)(\varepsilon_4^*\cdot k_3)\big] \\
& + (\varepsilon_3^*\cdot\varepsilon_4^*)\big[(\varepsilon_1\cdot k_3)(\varepsilon_2\cdot k_4)-(\varepsilon_1\cdot k_4)(\varepsilon_2\cdot k_3)\big] \\
& - (\varepsilon_2\cdot k_1)\big[(\varepsilon_1\cdot\varepsilon_3^*)(\varepsilon_4^*\cdot k_3)-(\varepsilon_1\cdot\varepsilon_4^*)(\varepsilon_3^*\cdot k_4)\big] \\
& - (\varepsilon_1\cdot k_2)\big[(\varepsilon_2\cdot\varepsilon_4^*)(\varepsilon_3^*\cdot k_4)-(\varepsilon_2\cdot\varepsilon_3^*)(\varepsilon_4^*\cdot k_3)\big]\Big\},
\end{aligned} \tag{10}$$

$$\begin{aligned}
\mathcal{M}_2 = {} & (\varepsilon_1\cdot\varepsilon_3^*)(\varepsilon_2\cdot\varepsilon_4^*)(s-u) \\
& - 4\Big\{(\varepsilon_1\cdot\varepsilon_3^*)\big[(\varepsilon_2\cdot k_3)(\varepsilon_4^*\cdot k_2)+(\varepsilon_2\cdot k_4)(\varepsilon_4^*\cdot k_3)\big] \\
& + (\varepsilon_2\cdot\varepsilon_4^*)\big[(\varepsilon_1\cdot k_2)(\varepsilon_3^*\cdot k_4)-(\varepsilon_1\cdot k_4)(\varepsilon_3^*\cdot k_2)\big] \\
& - (\varepsilon_1\cdot k_3)\big[(\varepsilon_3^*\cdot\varepsilon_4^*)(\varepsilon_2\cdot k_4)+(\varepsilon_2\cdot\varepsilon_3^*)(\varepsilon_4^*\cdot k_2)\big] \\
& - (\varepsilon_3^*\cdot k_1)\big[(\varepsilon_1\cdot\varepsilon_4^*)(\varepsilon_2\cdot k_4)+(\varepsilon_1\cdot\varepsilon_2)(\varepsilon_4^*\cdot k_2)\big]\Big\},
\end{aligned} \tag{11}$$

$$\mathcal{M}_3 = (\varepsilon_1\cdot\varepsilon_2)(\varepsilon_3^*\cdot\varepsilon_4^*)+(\varepsilon_1\cdot\varepsilon_3^*)(\varepsilon_2\cdot\varepsilon_4^*)-2(\varepsilon_1\cdot\varepsilon_4^*)(\varepsilon_2\cdot\varepsilon_3^*)\,, \tag{12}$$

$$\mathcal{M}_4 = (\varepsilon_1\cdot\varepsilon_2)(\varepsilon_3^*\cdot\varepsilon_4^*)\,, \tag{13}$$

$$\mathcal{M}_5 = (\varepsilon_1\cdot\varepsilon_3^*)(\varepsilon_2\cdot\varepsilon_4^*)\,. \tag{14}$$

For equal polarizations in the initial and final state, i.e. for $\lambda_1=\lambda_3$ and $\lambda_2=\lambda_4$, the lowest-order amplitude diverges for small momentum transfer t owing to the t-channel photon-exchange diagram. In fact, in this limit the lowest-order cross-section turns into the Rutherford cross-section $\propto 1/t^2 \propto 1/[p\sin(\theta/2)]^4$. If either $\lambda_1=\lambda_3$ or $\lambda_2=\lambda_4$, the cross-section has at most a $1/t$ singularity for small t, and for $\lambda_1\neq\lambda_3$ and $\lambda_2\neq\lambda_4$ it is regular.

Each longitudinal W boson enhances the individual matrix elements $\mathcal{M}_1$–$\mathcal{M}_5$ by a factor $\sqrt{s}/M_{\mathrm{W}}$. The cancellations guaranteed by gauge symmetry prevent the cross-section for longitudinal WW scattering from grossly violating unitarity at high energies. The gauge cancellations are demonstrated graphically in Fig. 2 for the total cross-section. The cross-section calculated from individual diagrams involving three- (a) or four-gauge-boson couplings (b) grows with s^3 for large s. Adding up all pure gauge-boson diagrams the leading terms cancel resulting in a cross-section $\propto s$. Including the Higgs-exchange diagrams, further cancellations take place such that the SM cross-section drops as $1/s$. The cancellations are already quite substantial at a few hundred GeV.

The unitarity cancellations ensure that all polarized cross-sections decrease at least as $1/s$ at high energies. The cross-sections with an odd number of longitudinal W bosons are suppressed by an additional factor M_{W}^2/s. The behaviour of various polarized cross-sections at high energies is listed in Table 1.

Polarization	$\sigma_{\mathrm{Born}} = \pi\alpha^2/s_{\mathrm{W}}^4 \cdot (\text{entry})$
LLLL	$\frac{1}{s}\left\{\frac{(M_{\mathrm{H}}^2+M_{\mathrm{Z}}^2)(2M_{\mathrm{Z}}^2L_c+M_{\mathrm{H}}^2c)}{4M_{\mathrm{W}}^4}+\frac{c\,(75-26c^2-c^4)}{48c_{\mathrm{W}}^4(1-c^2)}\right\}$
LLLT = LLTL = 2 LTLL = 2 TLLL	$-\frac{1}{s^2}\left\{\frac{(M_{\mathrm{H}}^2+4M_{\mathrm{W}}^2+M_{\mathrm{Z}}^2)^2L_c}{4M_{\mathrm{W}}^2} + \frac{c\left[3\left(M_{\mathrm{H}}^2+2(3M_{\mathrm{W}}^2+M_{\mathrm{Z}}^2)\right)^2-(6-c^2)(2M_{\mathrm{W}}^2+M_{\mathrm{Z}}^2)^2\right]}{12M_{\mathrm{W}}^2}\right\}$
LLTT = 4 TTLL	$\frac{1}{s}\frac{c\,(3+c^2)}{6}$
LTLT = TLTL	$\frac{1}{s}\left\{\frac{c\,(5-c^2)}{1-c^2}+2L_c\right\}$
LTTL = TLLT	$\frac{1}{s^3}\left\{[M_{\mathrm{H}}^4+M_{\mathrm{Z}}^4+2M_{\mathrm{H}}^2(8M_{\mathrm{W}}^2+M_{\mathrm{Z}}^2)]L_c+\frac{c\,(5-c^2)(M_{\mathrm{H}}^4+M_{\mathrm{Z}}^4)}{2(1-c^2)} + \frac{c\,(8M_{\mathrm{W}}^2+M_{\mathrm{Z}}^2)\left[18M_{\mathrm{H}}^2+(3+c^2)(8M_{\mathrm{W}}^2+M_{\mathrm{Z}}^2)\right]}{6}\right\}$
LTTT = TLTT = 2 TTLT = 2 TTTL	$-\frac{1}{s^2}M_{\mathrm{W}}^2(29c+3c^3+20L_c)$
TTTT	$\frac{1}{s}\left\{\frac{c\,(75-26c^2-c^4)}{3(1-c^2)}+8L_c\right\}$

Table 1: Leading terms for polarized integrated lowest-order cross-sections in the high-energy limit. Here $c=\cos\theta_{\mathrm{cut}}$, $L_c=\ln\frac{1-c}{1+c}$, and the relations between different polarizations in the left column are to be read, for instance, as $\sigma_{\mathrm{LTTT}}=2\sigma_{\mathrm{TTLT}}$, where the numerical prefactors originate from the different spin averages.

3.2 Numerical results

All following numerical results are obtained for an angular cut-off of $\theta_{\mathrm{cut}}=10°$ and for a Higgs-boson mass $M_{\mathrm{H}}=100\,\mathrm{GeV}$. This value is within the range allowed by precision data, which favour a light Higgs boson [14]. Since it lies below the threshold for $\mathrm{W^+W^-}\to\mathrm{W^+W^-}$ no Higgs resonance occurs.

In Fig. 3 the integrated lowest-order cross-section is displayed for various W polarizations. The curves nicely reflect the high-energy behaviour of the analytical expressions in Table 1. The cross-sections for the polarizations LLLL, TTTT, LTLT, and LTTL behave as $1/s$ at high energies, all others are suppressed by additional factors M_{W}^2/s. Owing to the $1/t$ pole, the cross-sections with equal initial- and final-state polarizations, LLLL, TTTT, and LTLT, are enhanced by a factor $1/(1-\cos^2\theta_{\mathrm{cut}})\approx 33$ for $\theta_{\mathrm{cut}}=10°$ and are therefore dominant. For these polarizations the contribution of the backward hemisphere to the integrated cross-section is less than 1% for energies above 1 TeV and at most 3% for lower energies. Note that the size of the corresponding integrated cross-sections strongly depends on the angular cut, θ_{cut}, because of the t-channel singularity.

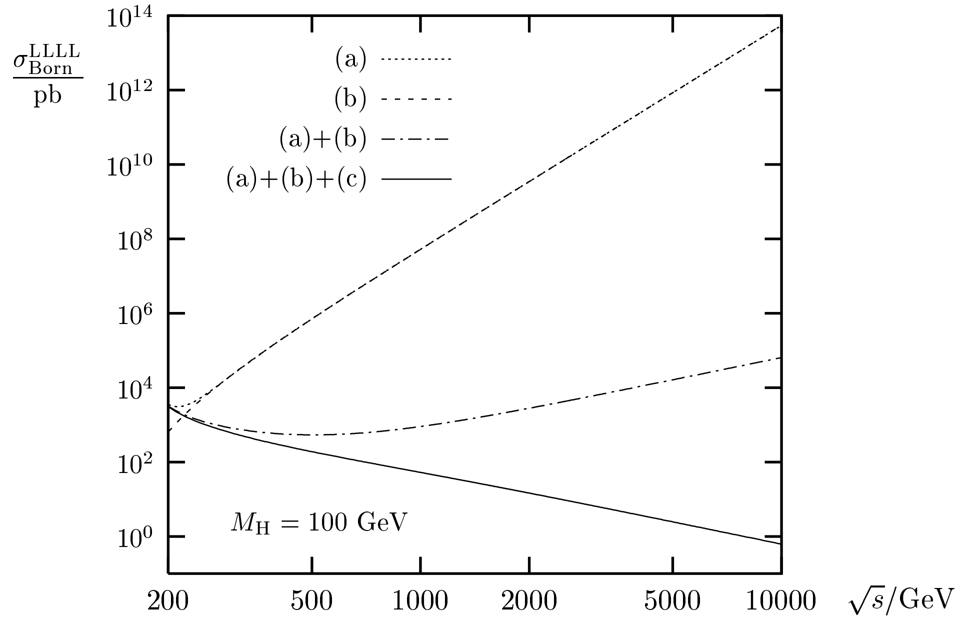

Figure 2: The cross-sections for longitudinal gauge-boson scattering resulting from subsets of the tree-level diagrams: (a) diagrams involving only three-gauge-boson couplings, (b) diagram involving only four-gauge-boson couplings, (c) diagrams involving Higgs bosons.

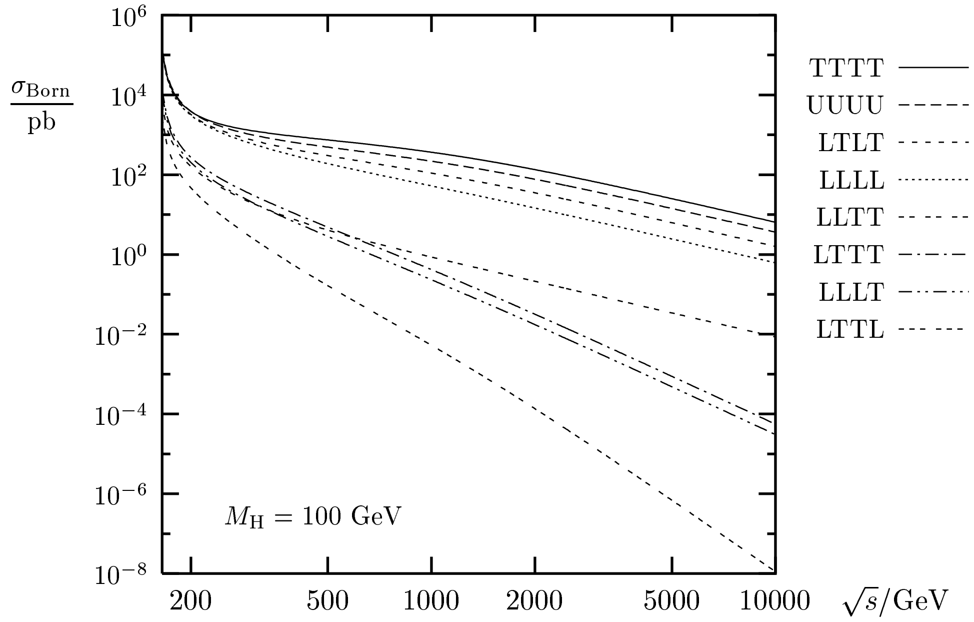

Figure 3: The integrated lowest-order cross-sections for various polarizations.

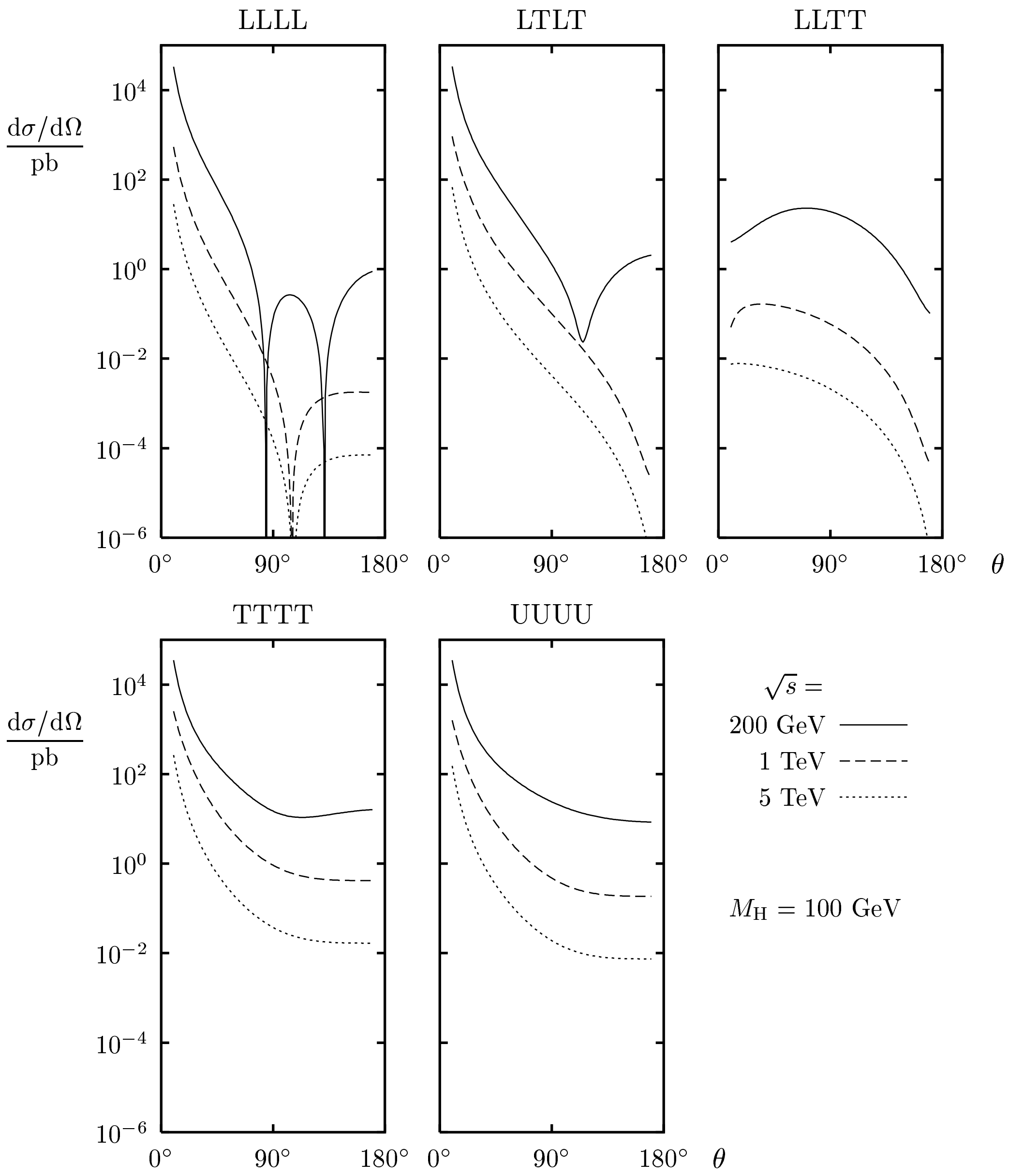

Figure 4: The differential lowest-order cross-sections for various polarizations at different energies.

In Fig. 4 the differential lowest-order cross-sections are shown for $\sqrt{s} = 200\,\mathrm{GeV}$, $1\,\mathrm{TeV}$, and $5\,\mathrm{TeV}$ for the dominating polarizations LLLL, LTLT, LLTT, TTTT, and for the unpolarized case UUUU. For all these polarizations except LLTT the curves display the strong forward peak resulting from the t-channel pole. The figures show that the main contributions to the unpolarized cross-section in backward direction come from completely transversally polarized bosons. The sharp dips in the longitudinal cross-section correspond to zeros in the amplitude. To be precise, the longitudinal cross-section is a rational function in t and has four such zeros. For $\sqrt{s} \lesssim 274\,\mathrm{GeV}$ two of these zeros and for $\sqrt{s} \gtrsim 274\,\mathrm{GeV}$ one of them lie in the physical region.

4 $\mathcal{O}(\alpha)$ corrections

4.1 Calculational framework

We have performed the calculation of the $\mathcal{O}(\alpha)$ radiative corrections in 't Hooft–Feynman gauge both in the conventional formalism and in the background-field formalism. Ultraviolet (UV) divergences are treated within dimensional regularization. We use the on-shell renormalization scheme [15], following the formulation worked out in Ref. [16] for the conventional formalism and in Ref. [17] for the background-field formalism. In the conventional formalism the field renormalization is fixed such that no external wave-function renormalization is needed. In the renormalization scheme introduced in Ref. [17] for the background-field method the field renormalization is determined by gauge invariance, and a non-trivial external wave-function renormalization is required, as explicitly described in Ref. [18].

Our calculation is based on the second of the two methods described in Ref. [13]. The Feynman diagrams are generated with *FeynArts* [19]. The resulting amplitudes are algebraically simplified with a combination of *Form* [20] and *Mathematica* and are then converted into a *Fortran* program. The tensor integrals are numerically reduced to scalar integrals, which are evaluated using the *FF* package [21].

4.2 Inventory

At one-loop level, roughly 1000 diagrams contribute to $\mathrm{W}^+\mathrm{W}^- \rightarrow \mathrm{W}^+\mathrm{W}^-$. The diagrams can be classified into self-energy corrections, vertex corrections, and box corrections. The self-energy corrections and the vertex corrections can be further divided into s- and t-channel contributions, the box corrections involve in addition u-channel contributions. The t-channel contributions can be obtained from the s-channel contributions via crossing, i.e. via the interchange of the outgoing W^- boson with the incoming W^+ boson.

In the following we list the Feynman graphs in the conventional formalism in 't Hooft–Feynman gauge. To avoid presenting hundreds of diagrams, similar diagrams have been combined. Each combination of particle labels on the internal lines corresponds to an extra diagram, where those have to be omitted that violate charge or lepton-number conservation or involve one of the following vertices: $\gamma\gamma HH$, $\gamma\gamma\chi\chi$, γZHH, $\gamma Z\chi\chi$, $W^+W^-\chi H$, χHH, $Z\chi\chi$, ZHH, $\gamma\chi\chi$, $\gamma\chi H$, γHH, $\gamma\nu\nu$, which do not exist in the SM. For example, diagram #1 of Fig. 5 represents a ϕ-loop contribution to the photon self-energy and to the γZ and $Z\gamma$ mixing, and ϕ-, χ-, and H-loop contributions to the Z-boson self-energy. If the charge flow in the internal lines is not indicated, it can take both directions (e.g. in diagram #5 in Fig. 5) or it is determined from the charges of the external W bosons (e.g. in diagram #2 in Fig. 6). In addition, fermionic diagrams are shown only for the first fermion generation.

The s-channel self-energy corrections are shown in Fig. 5. They consist of insertions of the Z-boson and photon self-energies and the γ–Z-boson mixing energy into diagram #1 of Fig. 1 and Higgs-boson self-energy insertions into diagram #4 of Fig. 1.

The s-channel vertex corrections consist of corrections to the γWW, ZWW and HWW vertices in diagrams #1 and #4 of Fig. 1. The corrections to the final-state vertices in these diagrams are displayed in Fig. 6.

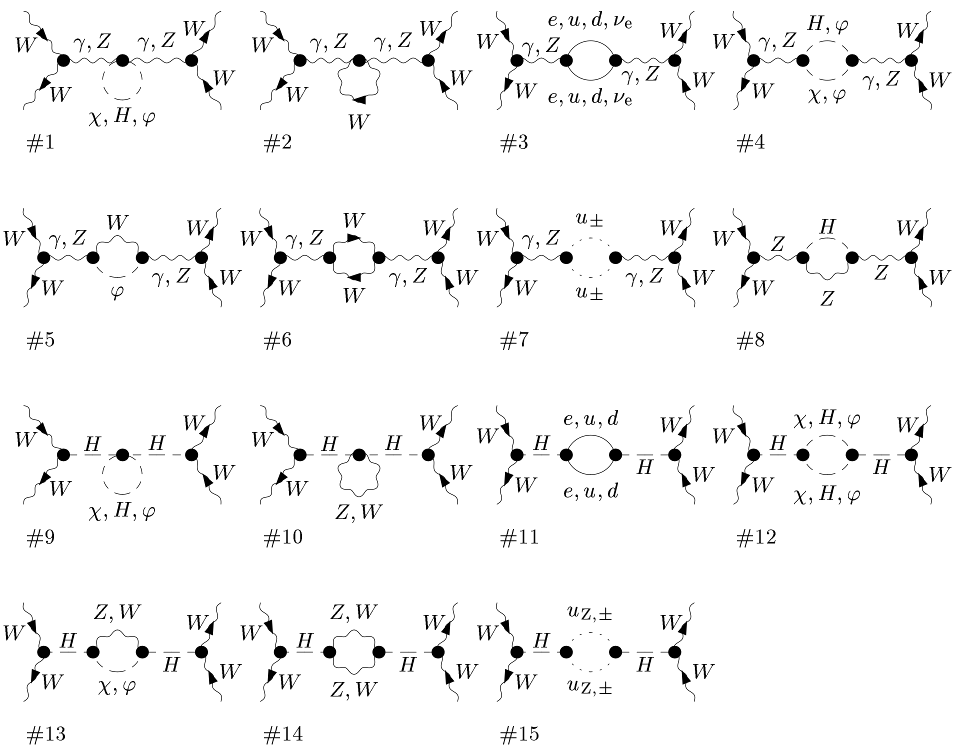

Figure 5: The s-channel self-energy diagrams.

The box diagrams are shown in Figs. 7, 8, and 9. While the t-channel boxes are obtained from the s-channel boxes via crossing, the u-channel boxes are different owing to the different charge flow. In particular, there are no fermionic u-channel diagrams. For this reason, the Landau singularity that appears in the corrections to ZZ $\to$ ZZ [13] does not show up in $\mathrm{W}^+\mathrm{W}^- \to \mathrm{W}^+\mathrm{W}^-$.

Apart from the virtual corrections, one has to take into account real soft-photon emission from the external W bosons in order to cancel the infrared (IR) divergences in the charge form factor. The IR divergences are regularized by a infinitesimal photon mass λ. In the soft-photon limit the cross-section for real photon emission is given by

$$\left(\frac{\mathrm{d}\sigma}{\mathrm{d}\Omega}\right)_{\mathrm{soft}} = \left(\frac{\mathrm{d}\sigma}{\mathrm{d}\Omega}\right)_{\mathrm{Born}} \delta_{\mathrm{soft}} \tag{15}$$

with the soft-photon correction factor

$$\delta_{\mathrm{soft}} = -\frac{e^2}{(2\pi)^3} \int_{k_0 \leqslant \Delta E} \frac{\mathrm{d}^3 k}{2k_0} \sum_{i,j=1}^{4} \frac{\pm Q_i Q_j \, (k_i \cdot k_j)}{(k_i \cdot k)(k_j \cdot k)} \bigg|_{k_0=\sqrt{\vec{k}^{\,2}+\lambda^2}} . \tag{16}$$

Here ΔE is the maximum energy of the emitted photons, $Q_i = \pm 1$ is the charge quantum number of the ith W boson, and the sign in front of the product $Q_i Q_j$ is '+' if particles i and j are both either incoming or outgoing and '$-$' otherwise.

The basic integrals needed for the soft-photon factor have been worked out, for in-

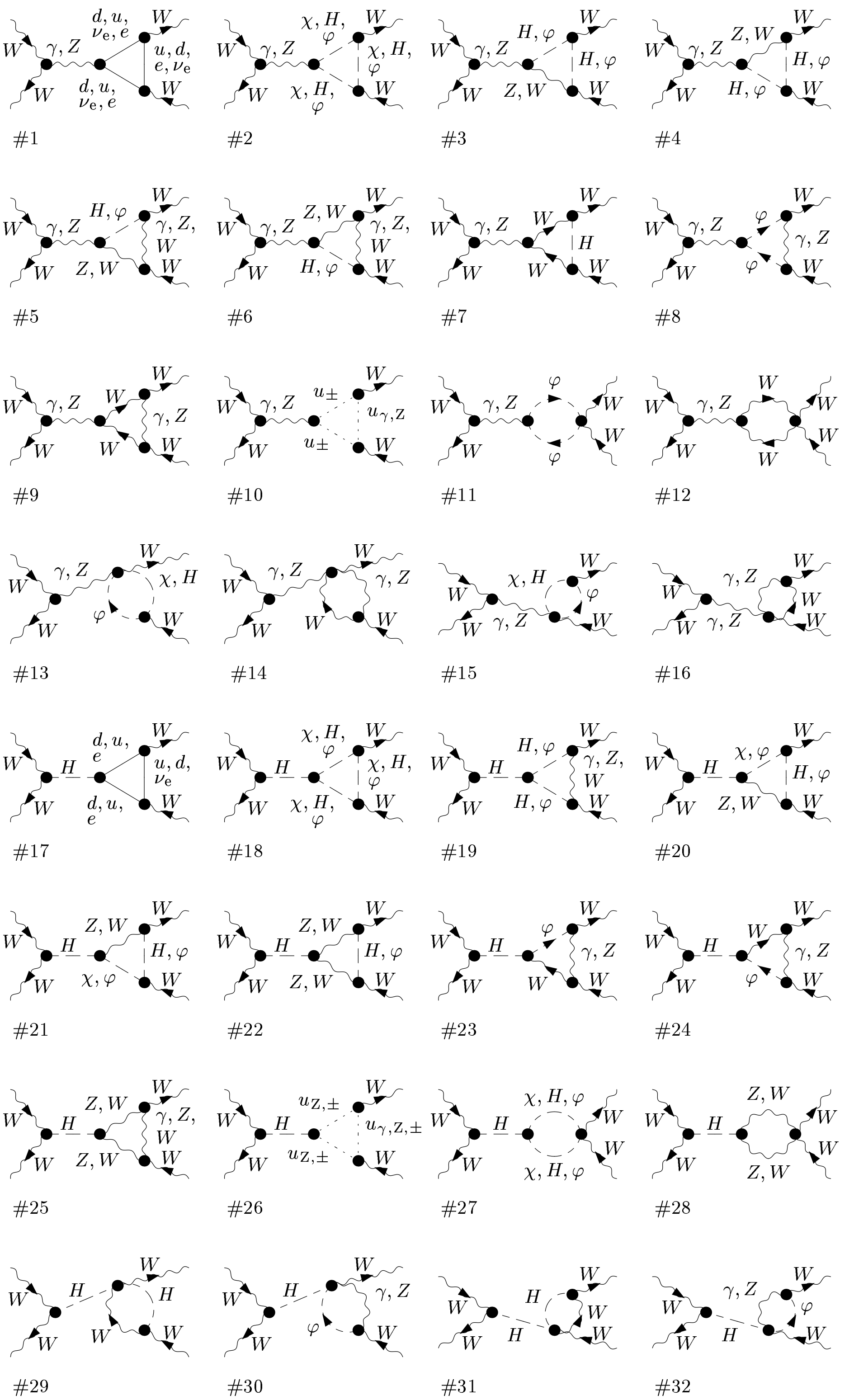

Figure 6: The s-channel vertex diagrams for the final-state vertex.

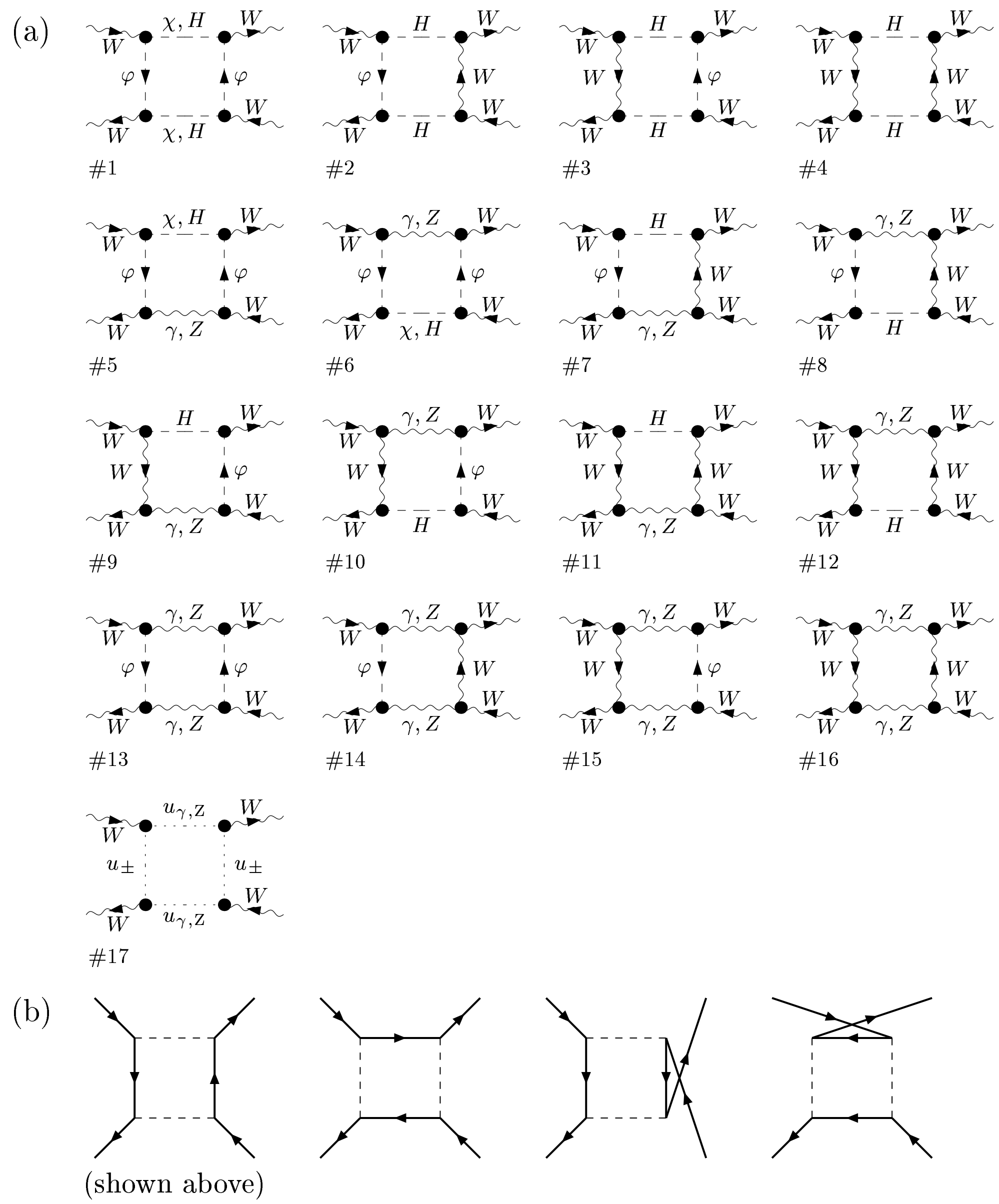

Figure 7: Genuine box diagrams that appear in the s, t, and u channel. Each diagram in (a) represents actually four diagrams with different charge flows shown in (b), i.e. one s-channel, one t-channel, and two u-channel diagrams.

stance, in Ref. [22]. For the case of $\mathrm{W^+W^-} \to \mathrm{W^+W^-}$ the soft-photon factor reads

$$
\begin{aligned}
\delta_{\mathrm{soft}} = -\frac{2\alpha}{\pi}\Bigg\{ & 2\ln\frac{2\Delta E}{\lambda} + \frac{E}{p}\ln\frac{E-p}{E+p} \\
& - (s-2M_{\mathrm{W}}^2)\,\mathcal{I}\Big(s+\sqrt{s(s-4M_{\mathrm{W}}^2)}\Big) \\
& - (2M_{\mathrm{W}}^2-t)\,\mathcal{I}\Big(4M_{\mathrm{W}}^2-t+\sqrt{t(t-4M_{\mathrm{W}}^2)}\Big) \\
& + (2M_{\mathrm{W}}^2-u)\,\mathcal{I}\Big(4M_{\mathrm{W}}^2-u+\sqrt{u(u-4M_{\mathrm{W}}^2)}\Big)\Bigg\},
\end{aligned}
\tag{17}
$$

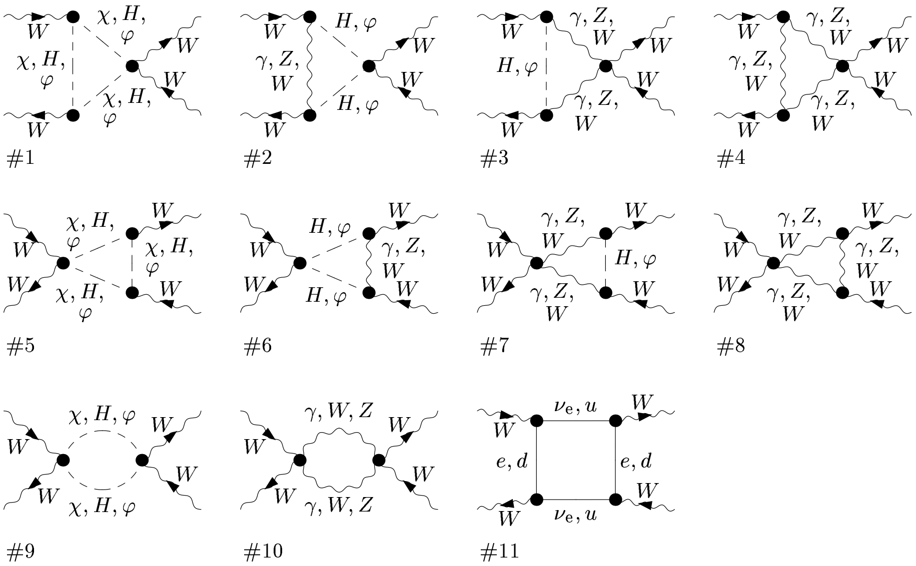

Figure 8: Further s-channel box diagrams. For every diagram there exists a t-channel analogue (obtained by exchanging the lower left and upper right leg).

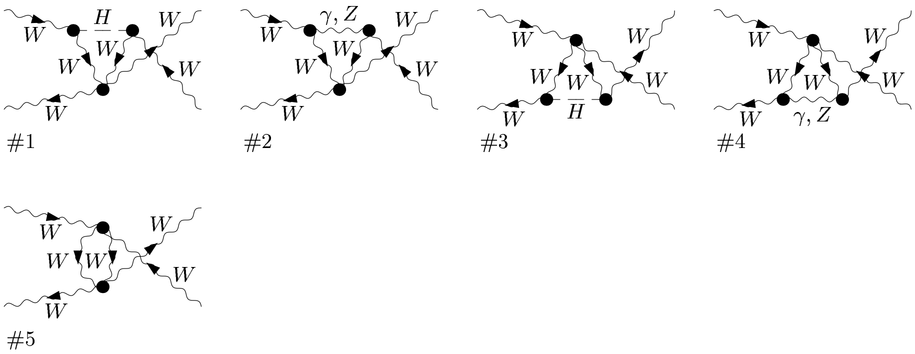

Figure 9: Further u-channel box diagrams.

where the function $\mathcal{I}(x)$ is defined as

$$
\begin{aligned}
\mathcal{I}(x) = \frac{2(x-2M_{\mathrm{W}}^2)}{x(x-4M_{\mathrm{W}}^2)} \Biggl\{ & 2\ln\frac{2\Delta E}{\lambda}\ln\frac{x-2M_{\mathrm{W}}^2}{2M_{\mathrm{W}}^2} \\
& + \mathrm{Li}_2\left(1-\frac{4E(E-p)}{x}\frac{x-2M_{\mathrm{W}}^2}{2M_{\mathrm{W}}^2}\right) - \mathrm{Li}_2\left(1-\frac{4E(E-p)}{x}\right) \\
& + \mathrm{Li}_2\left(1-\frac{4E(E+p)}{x}\frac{x-2M_{\mathrm{W}}^2}{2M_{\mathrm{W}}^2}\right) - \mathrm{Li}_2\left(1-\frac{4E(E+p)}{x}\right)\Biggr\}.
\end{aligned} \tag{18}
$$

4.3 Leading corrections

At low energies ($E \sim M_{\mathrm{W}}$) the electroweak radiative corrections are dominated by the universal corrections associated with the running of α and the ρ parameter. These effects are typically at the level of 10%. In this energy region no large logarithmic corrections associated with collinear photons appear in $\mathrm{W}^+\mathrm{W}^- \to \mathrm{W}^+\mathrm{W}^-$ because no light external particles are involved.

At high energies ($E \gg M_{\rm W}$) and for a light Higgs boson, the radiative corrections are dominated by corrections of the form $(\alpha/\pi)\ln(|x|/M_{\rm W}^2)\ln(|y|/M_{\rm W}^2)$, $x, y = s, t, u$, which originate from approximate IR and collinear singularities in the vertex and box diagrams.[1] These terms are are of the order of 10 and 20% at 1 and 10 TeV, respectively. At even higher energies these logarithms render the one-loop results useless and perturbation theory breaks down. In order to obtain sensible predictions for exclusive cross-sections beyond 10 TeV some kind of resummation of these logarithms is required. When considering more inclusive quantities and taking into account W-boson, Z-boson, and Higgs-boson bremsstrahlung, the $(\alpha/\pi)\ln(|x|/M_{\rm W}^2)\ln(|y|/M_{\rm W}^2)$ terms should drop out leaving leading terms of the form $(\alpha/\pi)\ln(|x|/M_{\rm W}^2)$.

If the Higgs boson is very heavy, additional large corrections appear. These corrections are, in particular, important for the scattering of longitudinal W bosons and have been extensively discussed in the literature [2,3,24]. In the limit $M_{\rm H}^2 \gg s \gg M_{\rm W}^2$, terms of the form $(\alpha/\pi s_{\rm W}^2)(|x|/M_{\rm W}^2)\ln(M_{\rm H}^2/|y|)$, $x, y = s, t, u$, which have been calculated in Refs. [2,24], dominate the relative corrections. For $s \gg M_{\rm H}^2 \gg M_{\rm W}^2$, on the other hand, the leading relative correction is provided by terms of the form $(\alpha/\pi s_{\rm W}^2)(M_{\rm H}^2/M_{\rm W}^2)\ln(|x|/M_{\rm H}^2)$. In this limit also the two-loop corrections are available [25]. The complete one-loop corrections proportional to $M_{\rm H}^2/M_{\rm W}^2$ to longitudinal W-boson scattering for $s, M_{\rm H}^2 \gg M_{\rm W}^2$ can be found in Ref. [3]. Finally, the leading logarithmic corrections of the form $(\alpha/\pi s_{\rm W}^2)\ln(M_{\rm H}^2/M_{\rm W}^2)$ in the limit $M_{\rm H}^2 \gg s, M_{\rm W}^2$ for the scattering of arbitrarily polarized W bosons are given in Ref. [26].

4.4 Checks of the calculation

Several cross-checks were performed to ascertain the correctness of our calculation. In particular, we checked

- the algebraic simplification of the Feynman diagrams by comparing the *Form* results with those obtained from *FeynCalc* [27] for selected diagrams (analytically),
- the numerical evaluation of the Feynman diagrams by comparing the evaluation of selected diagrams in *Fortran* and in *Mathematica* (numerically),
- the evaluation of the scalar and tensor one-loop integrals by comparing the results of the *FF* routines with own routines (numerically),
- the gauge independence of the results by comparing the results in conventional formalism and background-field formalism (numerically),
- the UV finiteness by proving independence of the scale parameter μ of dimensional regularization (analytically),
- the IR finiteness by testing independence of the regulator mass λ (numerically).

Numerical computations were done using extended precision (quadruple precision) with a mantissa of approximately 33 digits. The relative deviation between numerical results

[1]For the process $e^+e^- \to W^+W^-$ these leading terms can be read off from the high-energy expansion given in Ref. [23].

from different calculational methods was less than 10^{-16}. A double precision calculation is in general sufficient up to about 10 TeV. For higher energies the gauge cancellations become so large that double precision does not give reliable results any more.

5 Numerical results for the $\mathcal{O}(\alpha)$ corrections

5.1 Input parameters and definition of the corrected cross-section

For the calculations the following parameter set is used [28]:

$$
\begin{aligned}
\alpha^{-1} &= 137.0359895, & M_{\mathrm{Z}} &= 91.188\,\mathrm{GeV}, & M_{\mathrm{W}} &= 80.401\,\mathrm{GeV}, \\
m_{\mathrm{e}} &= 0.51099906\,\mathrm{MeV}, & m_{\mathrm{u}} &= 47.0\,\mathrm{MeV}, & m_{\mathrm{d}} &= 47.0\,\mathrm{MeV}, \\
m_{\mu} &= 105.658389\,\mathrm{MeV}, & m_{\mathrm{c}} &= 1.55\,\mathrm{GeV}, & m_{\mathrm{s}} &= 150\,\mathrm{MeV}, \\
m_{\tau} &= 1771.1\,\mathrm{MeV}, & m_{\mathrm{t}} &= 175.5\,\mathrm{GeV}, & m_{\mathrm{b}} &= 4.5\,\mathrm{GeV}.
\end{aligned}
\tag{19}
$$

The masses of the light quarks are adjusted such that the experimentally measured hadronic vacuum polarization is reproduced [29]. As before, a Higgs-boson mass of $M_{\mathrm{H}} = 100\,\mathrm{GeV}$ is used, and the integrated cross-sections are evaluated for an angular cut $\theta_{\mathrm{cut}} = 10°$.

All cross-sections discussed in the following are calculated by replacing the matrix element squared in (4) by

$$
|\mathcal{M}|^2 \to |\mathcal{M}_{\mathrm{Born}}|^2 \,(1+\delta_{\mathrm{soft}}) + 2\,\mathrm{Re}(\mathcal{M}^*_{\mathrm{Born}}\delta\mathcal{M})\ , \tag{20}
$$

where $\delta\mathcal{M}$ is the sum of the one-loop Feynman diagrams, and δ_{soft} the soft-photon correction factor (16). Note that this yields the cross-section including all $\mathcal{O}(\alpha)$ corrections but neglecting all $\mathcal{O}(\alpha^2)$ corrections.

In the soft-photon approximation the corrections depend on the soft-photon cut-off energy ΔE via logarithms of the form $\ln(\Delta E/E)$. For small ΔE, where the soft-photon approximation is valid, these terms give rise to large corrections, which are, however, cancelled if hard-photon bremsstrahlung is taken into account. In order to avoid artificially large soft-photon effects, we have chosen to discard all terms involving $\ln(\Delta E/E)$ in the corrections.[2] The elimination of the cut-off-dependent terms can be simply achieved by choosing $\Delta E = E$. The corrections defined in this way can be viewed as a suitable measure of the weak corrections, which cannot be separated from the electromagnetic corrections on the basis of Feynman diagrams in a gauge-invariant way [11].

5.2 Total cross-sections

In Fig. 10, the integrated cross-sections in lowest order and including $\mathcal{O}(\alpha)$ corrections as well as the relative $\mathcal{O}(\alpha)$ corrections are plotted for the dominant polarizations LLLL, LTLT, LLTT, TTTT, and UUUU. For small energies the corrections are positive and roughly 10%. With increasing energy the corrections become large and negative and reach the order of the lowest-order cross-sections around 10 TeV. The large corrections at high energies originate from logarithms of the form $\alpha/\pi \ln^2(s/M_{\mathrm{W}}^2)$, which are additionally enhanced by numerical factors.

[2] Of course, these terms have to be reinstalled in a complete calculation involving hard-photon bremsstrahlung.

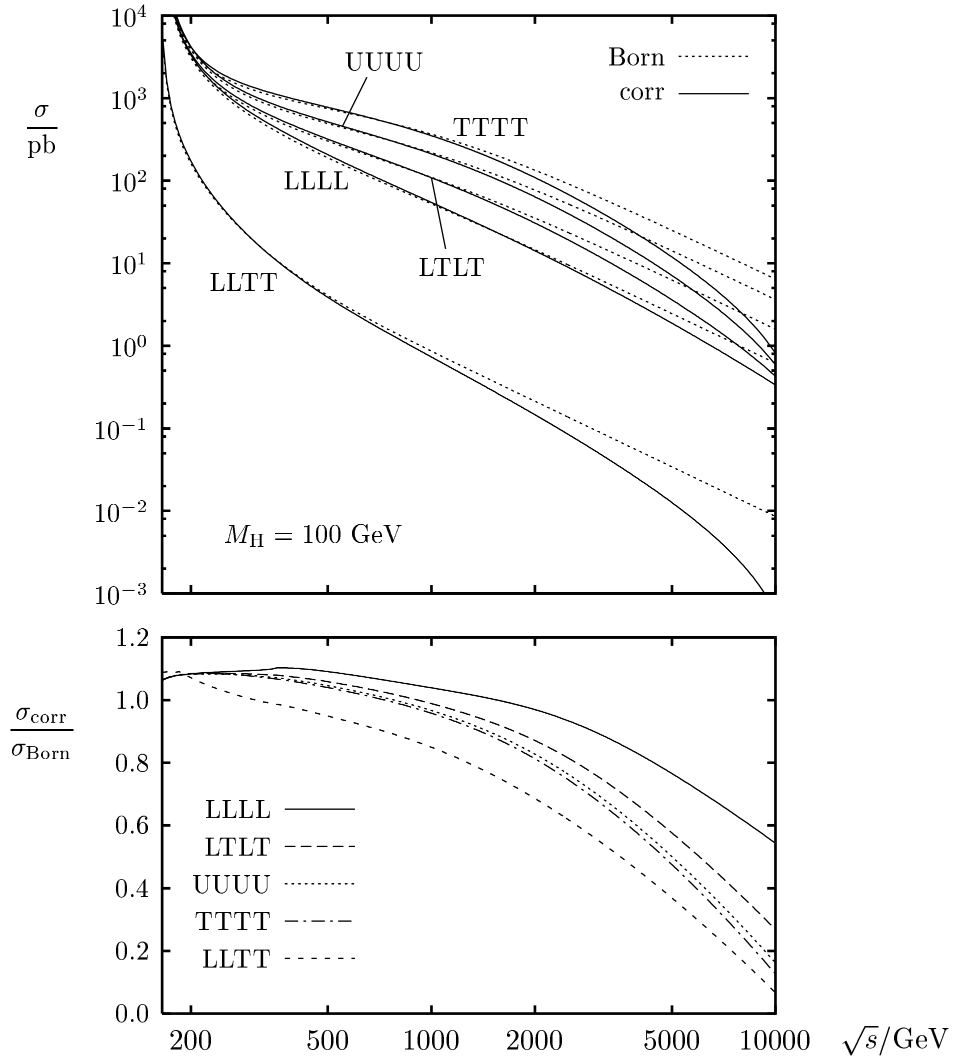

Figure 10: Upper plot: The integrated cross-sections for the dominant polarizations in lowest order (Born) and including the $\mathcal{O}(\alpha)$ corrections (corr). Lower plot: Relative corrections for the same polarizations.

5.3 Differential cross-sections

The lowest-order and corrected differential cross-sections for the dominant polarizations LLLL, LTLT, LLTT, TTTT, and UUUU are shown in Fig. 11 for $\sqrt{s} = 200\,\text{GeV}$, $1\,\text{TeV}$, and $5\,\text{TeV}$. The corrections are small at low energies for all scattering angles but get large at high energies, in particular in the backward direction. This is due to the fact that the contributions of the u-channel box diagrams to the cross-sections involve terms that behave as $1/|u|$ for $M_{\text{W}}^2 \ll |u| \ll s$ and approach a constant of the order of $1/M_{\text{W}}^2$ for $|u| \ll M_{\text{W}}^2$, while the lowest-order cross-sections are of order $1/s$ for $|u| \ll s$. Hence the relative corrections in the backward direction are typically enhanced by a factor $s/|u|$ compared with the corrections in forward direction or to the total cross-section and can easily reach 100% at several TeV. Since $|\delta\mathcal{M}|^2$ is missing in (20), the cross-section can formally become even negative in this case. By including $|\delta\mathcal{M}|^2$, the quality of the predic-

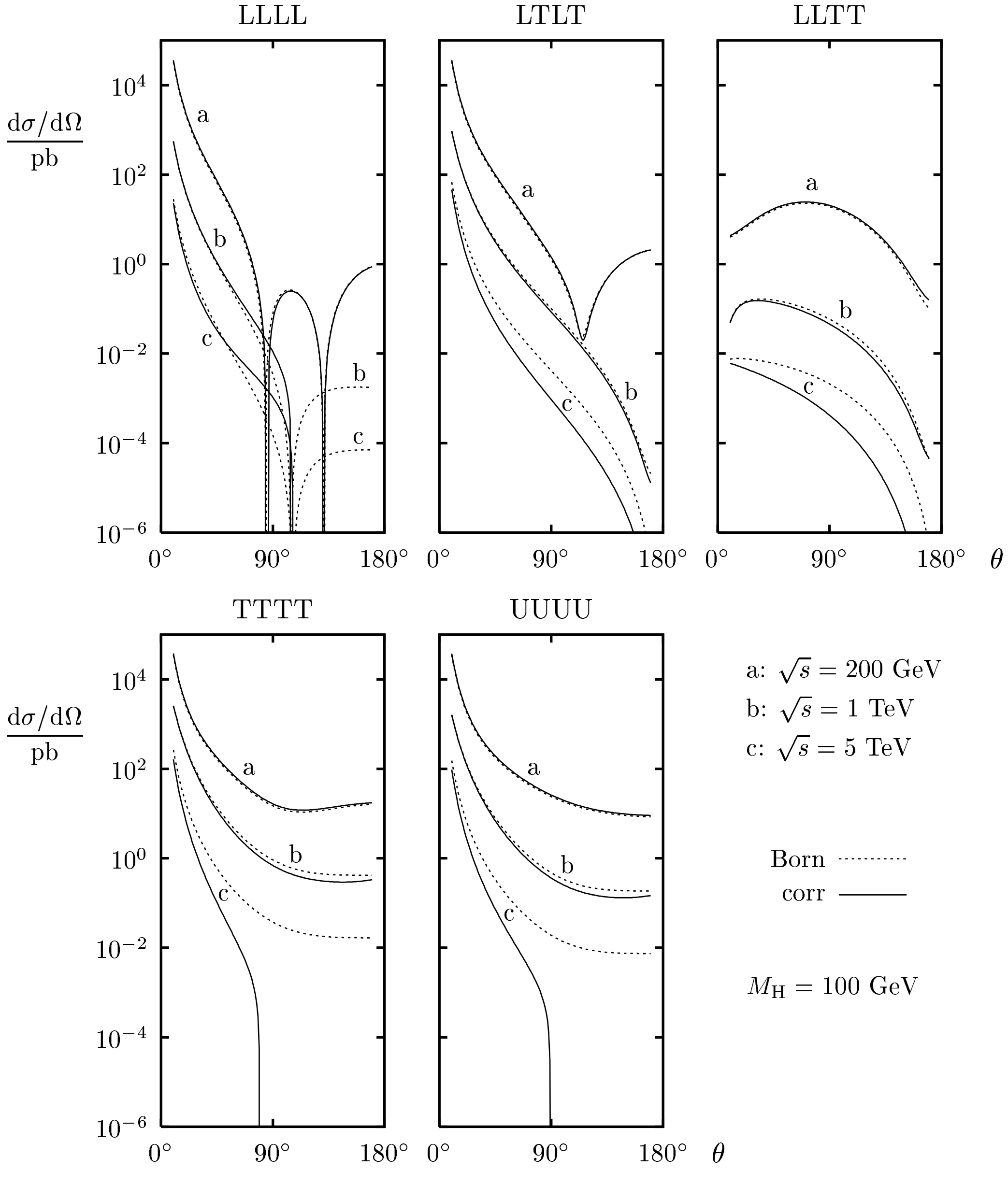

Figure 11: The differential cross-sections for the dominant polarizations at $\sqrt{s} = 200\,\mathrm{GeV}$, $1\,\mathrm{TeV}$, and $5\,\mathrm{TeV}$ in lowest order (Born) and including the $\mathcal{O}(\alpha)$ corrections (corr). Note that in some regions of phase space the corrected cross-sections become formally negative and are therefore not visible in these logarithmic plots.

tions can in general be improved, but for $\mathrm{W^+W^-} \to \mathrm{W^+W^-}$ this leads to problems, which are discussed in Section 6. Here, we ignore $|\delta\mathcal{M}|^2$ and the resulting wrong predictions for high energies and large scattering angles, since the cross-sections are small in this region, and, as has been stated above, the total cross-section is dominated by the forward hemisphere. The large corrections in the backward direction do not indicate a breakdown of perturbation theory because no additional enhancement factors s/u should appear in higher orders.

5.4 Accuracy of the equivalence-theorem predictions

The calculations of enhanced corrections to longitudinal gauge-boson scattering [2] usually have been done with the help of the equivalence theorem (ET) [10]. When using the ET in higher-order calculations one has to be careful to include all correction factors that result from renormalization and amputation [30]. This is particularly easy within the BFM [18], where the matrix elements for external longitudinal vector bosons are directly obtained from the amputated Green functions with the corresponding would-be Goldstone-boson fields multiplied with the wave-function renormalization constants of the gauge bosons.

We calculated the matrix element for $\varphi^+\varphi^- \to \varphi^+\varphi^-$ to one-loop order in the BFM and from this the ET prediction for the cross-section for $\mathrm{W}_\mathrm{L}^+\mathrm{W}_\mathrm{L}^- \to \mathrm{W}_\mathrm{L}^+\mathrm{W}_\mathrm{L}^-$

$$\left(\frac{\mathrm{d}\sigma}{\mathrm{d}\Omega}\right)_{\mathrm{ET}} = \frac{1}{64\pi^2 s}\Biggl[\left|\mathcal{M}_{\mathrm{Born}}^{\varphi^+\varphi^-\to\varphi^+\varphi^-}\right|^2(1+\delta_{\mathrm{soft}}) \\ + 2\,\mathrm{Re}\Bigl\{\bigl(\mathcal{M}_{\mathrm{Born}}^{\varphi^+\varphi^-\to\varphi^+\varphi^-}\bigr)^*\delta\mathcal{M}^{\varphi^+\varphi^-\to\varphi^+\varphi^-}\Bigr\}\Biggr]. \quad (21)$$

Since $\varphi^+\varphi^- \to \varphi^+\varphi^-$ and $\varphi^+\varphi^- \to \varphi^+\varphi^-\gamma$ are no physical processes, the cross-section (21) is not well-defined at finite energies. The ET is valid only for high energies and guarantees (21) to provide a sensible cross-section only in the high-energy limit, i.e. up to terms of order M_W/E. In fact, at finite energies (21) is gauge-dependent and the IR singularities between the virtual and real corrections do not cancel exactly. In the analytic results, which are obtained for an infinitesimal photon mass λ, terms proportional to $(M_\mathrm{W}/E)\ln(\lambda^2/s)$ and gauge-dependent terms proportional to (M_W/E) remain. In order to avoid an enhancement of the IR-singular terms, we have set the photon mass equal to the energy of the W bosons, $\lambda = E$, in the numerical evaluation. This ensures that the artificial IR-singular logarithms do not lead to enhanced contributions. Since also the soft-photon correction factor corresponding to $\varphi^+\varphi^- \to \varphi^+\varphi^-$ is gauge-dependent we have chosen to use directly the soft-photon correction factor for $\mathrm{W}^+\mathrm{W}^- \to \mathrm{W}^+\mathrm{W}^-$. We stress that despite the gauge-dependences and the IR-singularities contained in (21), our results are valid at the same level as all ET results, i.e. up to terms of order M_W/E.

In order to improve the accuracy of the ET calculation we combine the lowest-order cross-section for $\mathrm{W}_\mathrm{L}^+\mathrm{W}_\mathrm{L}^- \to \mathrm{W}_\mathrm{L}^+\mathrm{W}_\mathrm{L}^-$ with the $\mathcal{O}(\alpha)$ corrections from $\varphi^+\varphi^- \to \varphi^+\varphi^-$ as follows

$$\left(\frac{\mathrm{d}\sigma}{\mathrm{d}\Omega}\right)_{\mathrm{mixed}} = \frac{1}{64\pi^2 s}\Biggl[\left|\mathcal{M}_{\mathrm{Born}}^{\mathrm{W}_\mathrm{L}^+\mathrm{W}_\mathrm{L}^-\to\mathrm{W}_\mathrm{L}^+\mathrm{W}_\mathrm{L}^-}\right|^2 + \left|\mathcal{M}_{\mathrm{Born}}^{\varphi^+\varphi^-\to\varphi^+\varphi^-}\right|^2\delta_{\mathrm{soft}} \\ + 2\,\mathrm{Re}\Bigl\{\bigl(\mathcal{M}_{\mathrm{Born}}^{\varphi^+\varphi^-\to\varphi^+\varphi^-}\bigr)^*\delta\mathcal{M}^{\varphi^+\varphi^-\to\varphi^+\varphi^-}\Bigr\}\Biggr]. \quad (22)$$

In this way the error originating from the use of the ET enters only via the $\mathcal{O}(\alpha)$ corrections.

The accuracy of the ET predictions for the scattering of longitudinal W bosons is investigated in Fig. 12 and Table 2. We show the lowest-order cross-section for $\varphi^+\varphi^- \to \varphi^+\varphi^-$ normalized to the lowest-order cross-section for $\mathrm{W}_\mathrm{L}^+\mathrm{W}_\mathrm{L}^- \to \mathrm{W}_\mathrm{L}^+\mathrm{W}_\mathrm{L}^-$ and the corrected

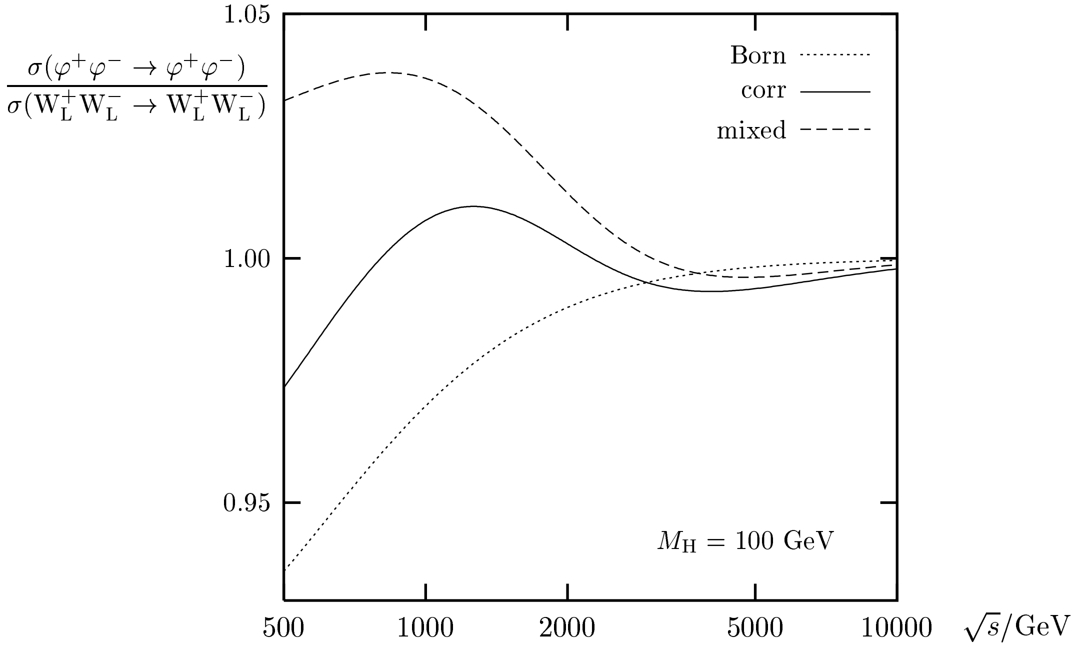

Figure 12: Ratio of the ET predictions for $W_L^+W_L^- \to W_L^+W_L^-$ and the direct calculation. "Born" and "corr" label the ratios of the tree-level and $\mathcal{O}(\alpha)$-corrected cross-sections, respectively. For the curve marked "mixed" the ET is used only for the corrections [cf. (22)].

	$\frac{\sigma(\varphi^+\varphi^- \to \varphi^+\varphi^-)}{\sigma(W_L^+W_L^- \to W_L^+W_L^-)} - 1$		
$\sqrt{s}$	Born	corr	mixed
500 GeV	−6.4%	−2.7%	3.2%
1 TeV	−3.0%	0.8%	3.7%
2 TeV	−1.0%	0.3%	1.3%
5 TeV	−0.2%	−0.6%	−0.4%
10 TeV	−0.0%	−0.2%	−0.1%

Table 2: Relative deviations of the ET predictions for $W_L^+W_L^- \to W_L^+W_L^-$.

cross-section calculated from the ET according to (21) and according to the improved formula (22), both normalized to the corrected cross-section for $W_L^+W_L^- \to W_L^+W_L^-$. For $\sqrt{s} \gtrsim 500\,\text{GeV}$ the deviations are all below 7% and become smaller at higher energies. Above about 2 TeV they are less than 1%. At high energies, where the ET is valid, the approximation (22) is in fact better than the pure ET prediction.

6 Difficulties beyond $\mathcal{O}(\alpha)$ accuracy

In Section 5 we found that the $\mathcal{O}(\alpha)$ corrections become of the order of the lowest-order cross-section for high energies. In this case higher-order corrections are required in order to arrive at a meaningful prediction. If the importance of the $\mathcal{O}(\alpha)$ corrections is due to a suppression of the lowest-order cross-section, as it happens for $W^+W^- \to W^+W^-$

at large scattering angles and high energies, it is appropriate to include the square of the $\mathcal{O}(\alpha)$ corrections, i.e. to calculate the cross-section via

$$\frac{\mathrm{d}\sigma}{\mathrm{d}\Omega} = \frac{1}{64\pi^2 s} \left|\mathcal{M}_{\mathrm{Born}} + \delta\mathcal{M}\right|^2 . \tag{23}$$

Because the interferences of the genuine $\mathcal{O}(\alpha^2)$ matrix element with the lowest-order matrix element are suppressed with the lowest-order cross-section, this gives a reasonable (leading-order) prediction, which is usually sufficient as the cross-section is suppressed. This recipe has for example been applied in the case of $\mathrm{ZZ} \to \mathrm{ZZ}$ [13].

Since for $\mathrm{W}^+\mathrm{W}^- \to \mathrm{W}^+\mathrm{W}^-$ this approach leads to severe problems, it was not used in this paper.

The first problem is due to the charge of the W boson. It gives rise to photonic corrections that render the matrix element for the process $\mathrm{W}^+\mathrm{W}^- \to \mathrm{W}^+\mathrm{W}^-$ IR-singular. In order to cancel the IR singularities one has to add real soft-photon radiation. The cancellation of the IR singularities takes place order by order. Including $|\delta\mathcal{M}|^2$ would thus require to take into account all virtual and real $\mathcal{O}(\alpha^2)$ corrections. Since the IR-singular corrections are proportional to the lowest-order matrix element and thus suppressed, an approximate result could nevertheless be obtained by including the real $\mathcal{O}(\alpha)$ corrections appropriately when squaring the matrix element. The error introduced by this effective treatment of the real corrections is of the order of the neglected $\mathcal{O}(\alpha^2)$ corrections.

The second, more severe difficulty is closely related to the instability of the W boson. When calculating the one-loop diagrams for $\mathrm{W}_\mathrm{L}^+\mathrm{W}_\mathrm{L}^- \to \mathrm{W}_\mathrm{L}^+\mathrm{W}_\mathrm{L}^-$ one finds that not all terms proportional to s cancel. The left-over terms proportional to s in the unrenormalized amplitude can be expressed in terms of the transverse W self-energy:

$$\delta\mathcal{M}^{\mathrm{unren.}}_{\mathcal{O}(s)} = \frac{4\pi\alpha}{s_\mathrm{W}^2}\cos^2\frac{\theta}{2}\frac{s}{M_\mathrm{W}^2}\frac{\Sigma_\mathrm{T}^W(M_\mathrm{W}^2)}{M_\mathrm{W}^2} . \tag{24}$$

The counter terms, in fact only the W-mass counter term $\delta M_\mathrm{W}^2 = \mathrm{Re}\,\Sigma_\mathrm{T}^W(M_\mathrm{W}^2)$ (and the derived counter term for the weak mixing angle δc_W^2), yield a similar contribution with opposite sign. When adding these contributions, the real part of $\delta\mathcal{M}^{\mathrm{unren.}}_{\mathcal{O}(s)}$ is exactly cancelled but the imaginary part survives. As a consequence the imaginary part of the one-loop matrix element for $\mathrm{W}_\mathrm{L}^+\mathrm{W}_\mathrm{L}^- \to \mathrm{W}_\mathrm{L}^+\mathrm{W}_\mathrm{L}^-$ grows with s and therefore would violate unitarity if taken into account. Because the lowest-order matrix element is real as long as no Higgs resonance is present, this does not affect the $\mathcal{O}(\alpha)$ corrections to the cross-section. However, in higher orders or if the Higgs-boson width has to be included the imaginary part becomes relevant and the perturbative evaluation of corrections to $\mathrm{W}_\mathrm{L}^+\mathrm{W}_\mathrm{L}^- \to \mathrm{W}_\mathrm{L}^+\mathrm{W}_\mathrm{L}^-$ for on-real-mass-shell external W bosons breaks down. This statement holds for the usual approach where the external W bosons are treated as stable particles with a real mass, i.e. where the corresponding momenta squared are set equal to the real W-boson mass squared.

The reason for the breakdown becomes apparent by noting that the unitarity-violating term can be written as

$$\delta\mathcal{M}_{\mathcal{O}(s)} = \frac{4\pi\alpha}{s_\mathrm{W}^2}\cos^2\frac{\theta}{2}\frac{s}{M_\mathrm{W}^2}\frac{\mathrm{i}\,\mathrm{Im}\,\Sigma_\mathrm{T}^W(M_\mathrm{W}^2)}{M_\mathrm{W}^2} = \mathrm{i}\frac{4\pi\alpha}{s_\mathrm{W}^2}\cos^2\frac{\theta}{2}\frac{s}{M_\mathrm{W}^2}\frac{\Gamma_\mathrm{W}}{M_\mathrm{W}} , \tag{25}$$

i.e. it is proportional to the (lowest-order) decay width of the W boson. This result shows that the problem is due to the instability of the W bosons, which is inherent in the one-loop calculation. It points to the fact that S-matrix elements for unstable external particles are not well-defined.

From the previous considerations it is clear that the unitarity-violating terms would cancel if the W-boson-mass counter term were complex, i.e. if renormalization would also compensate the imaginary part of the W self-energy. Since the bare W-boson mass is real, this can only be achieved if the renormalized W-boson mass (and the renormalized weak mixing angle) become complex.

Let us consider the matrix element in this renormalization scheme including $\mathcal{O}(\alpha)$ corrections. In the one-loop part and in the counter-term part, which are of order α, the renormalized parameters can be replaced by bare parameters and all unitarity-violating terms cancel out. In the tree-level matrix element, however, the complex renormalized parameters lead to unitarity-violating terms (if it is calculated for $k_i^2 = M_{\mathrm{W}}^2$). This reflects the fact that a change in renormalization scheme in an $\mathcal{O}(\alpha)$ calculation cannot eliminate $\mathcal{O}(\alpha)$ corrections but only reshuffle them. However, if we evaluate the matrix element for complex external momenta squared, $k_i^2 = M_{\mathrm{W}}^2 - \mathrm{i}M_{\mathrm{W}}\Gamma_{\mathrm{W}}$, all unitarity-violating terms cancel in the tree-level part, and the loop and counter-term parts are not changed (up to terms of order α^2) with respect to the evaluation with real external momenta squared, $k_i^2 = M_{\mathrm{W}}^2$. As a result, we find that the matrix element for $\mathrm{W}_{\mathrm{L}}^+\mathrm{W}_{\mathrm{L}}^- \to \mathrm{W}_{\mathrm{L}}^+\mathrm{W}_{\mathrm{L}}^-$ including $\mathcal{O}(\alpha)$ corrections respects unitarity if the squares of the external momenta are equal to the physical complex masses, but violates unitarity for real "on-shell" external momenta. This result is independent of the renormalization scheme, and holds, in particular, in the usual on-shell scheme. Our findings are in accordance with the fact that gauge invariance and unitarity of S-matrix elements require the momenta of the external particles to be on the mass shell, i.e. on the complex mass shell for unstable particles. They indicate that the natural generalization of S-matrix elements for unstable particles are the multiple residues at the physical (complex) poles of the external particles (compare Ref. [31]).

When calculating the corrections to $\mathrm{W}_{\mathrm{L}}^+\mathrm{W}_{\mathrm{L}}^- \to \mathrm{W}_{\mathrm{L}}^+\mathrm{W}_{\mathrm{L}}^-$ via the ET, no unitarity-violating terms appear. A closer look reveals that the validity of the ET demands external W bosons to be on their mass shell. Beyond $\mathcal{O}(\alpha)$ this requires the squares of the external momenta to be complex. For real external on-shell momenta the ET is not valid beyond $\mathcal{O}(\alpha)$.

The approach described above requires to consider matrix elements for complex external momenta squared. However, the momenta of physical particles are always real, even if these particles appear only as resonances in some process. Since it is not clear how to relate the physical real momenta to appropriate complex momenta we have not pursued this approach any further. The definition of S-matrix elements for unstable external particles remains an unsolved problem.

The only fully consistent way to calculate corrections to longitudinal W-boson scattering beyond $\mathcal{O}(\alpha)$ seems to be the evaluation of a physical process, e.g. $\mathrm{e}^+\mathrm{e}^- \to \mathrm{W}^+\mathrm{W}^- \to \mathrm{W}^+\mathrm{W}^- \to 4$ fermions, or at least the resonant contributions to this process. This is beyond the scope of this paper.

7 Conclusions

The scattering of the weak gauge bosons is an extremely useful tool for the investigation of the non-abelian gauge sector and the symmetry-breaking sector of the electroweak interaction. To lowest order these reactions involve only interactions between gauge and scalar bosons and, therefore, depend very sensitively on these couplings. Owing to its large cross-section, a particularly interesting process in this class is the scattering of charged W bosons, $W^+W^- \to W^+W^-$.

This process is known in the literature including only the leading corrections in the limit of high energies and large Higgs-boson masses. In this paper we have extended these results by calculating the complete virtual and soft-photonic $\mathcal{O}(\alpha)$ corrections to the amplitudes for $W^+W^- \to W^+W^-$ as predicted by the electroweak Standard Model.

The cross-sections with equal initial- and final-state polarizations exhibit a $1/t^2$ singularity resulting from the t-channel photon-exchange diagram and are therefore dominant. The corresponding $\mathcal{O}(\alpha)$ corrections are typically of the order of 10% for energies below roughly 2 TeV, grow with energy, and reach the order of the lowest-order cross-section at several TeV. The corrections become particularly large in the backward direction, where the cross-sections are relatively small. At energies beyond 10 TeV the one-loop calculation becomes unreliable and a resummation of the leading corrections or the inclusion of real massive boson emission is required.

The predictions of the equivalence theorem, which relates the scattering amplitudes of longitudinally polarized gauge bosons with those of the unphysical Goldstone-boson fields, have been compared with the direct calculation at the level of the $\mathcal{O}(\alpha)$ corrections and for a light Higgs boson. For energies above 500 GeV the deviations are below 7%, above about 2 TeV they are less than 1%.

We have found that the calculation of radiative corrections to the scattering of on-real-mass-shell longitudinal W bosons, i.e. to $W_L^+W_L^- \to W_L^+W_L^-$ in the usual sense, becomes inconsistent beyond $\mathcal{O}(\alpha)$. More precisely, the imaginary part of the one-loop matrix element gets a unitarity-violating contribution proportional to the W-boson width. This contribution does not affect the $\mathcal{O}(\alpha)$ corrections to the cross-section as long as no Higgs resonance appears. It becomes problematic as soon as the imaginary part of the matrix element enters an observable, i.e. if $\mathcal{O}(\alpha^2)$ corrections to the cross-section or the finite width of the Higgs boson are included. This result points to the fact that S-matrix elements for unstable external particles are not well-defined. For a consistent evaluation, the instability of the W bosons has to be taken into account properly. This seems to be only possible when considering a full process with stable initial- and final-state particles that involve $W_L^+W_L^- \to W_L^+W_L^-$ as an enhanced contribution.

Acknowledgements

We thank M. Böhm and S. Dittmaier for useful discussions.

References

[1] D.A. Dicus and V.S. Mathur, *Phys. Rev.* **D7** (1973) 3111;
B.W. Lee, C. Quigg and H.B. Thacker, *Phys. Rev.* **D16** (1977) 1519.

[2] S. Dawson and S. Willenbrock, *Phys. Rev. Lett.* **62** (1989) 1232;
G. Passarino, *Nucl. Phys.* **B343** (1990) 31;
M. Veltman and F. Yndurain, *Nucl. Phys.* **B325** (1989) 1.

[3] S. Dawson and S. Willenbrock, *Phys. Rev.* **D40** (1989) 2880;
S.N. Gupta, J.M. Johnson and W.W. Repko, *Phys. Rev.* **D48** (1993) 2083.

[4] R. Bouamrane, in: *Radiative Corrections: Results and Perspectives*, eds. N. Dombey and F. Boudjema, Plenum Press, New York (1990) 533;
S. Dawson and G. Valencia, *Nucl. Phys.* **B348** (1991) 23.

[5] J. Bagger, S. Dawson and G. Valencia, *Nucl. Phys.* **B399** (1993) 364;
I. Kuss and E. Nuss, BI-TP 97/16, hep-ph/9706406.

[6] V. Barger, K. Cheung, T. Han and R.J.N. Phillips, *Phys. Rev.* **D42** (1990) 3052;
J. Bagger et al., *Phys. Rev.* **D49** (1994) 1246 and *Phys. Rev.* **D52** (1995) 3878;
S.N. Gupta, J.M. Johnson, G.A. Ladinsky and W.W. Repko, *Phys. Rev.* **D53** (1996) 4897.

[7] W. Beenakker, *Acta Phys. Polon.* **B28** (1997) 1461;
E. Boos et al., DESY-96-256, hep-ph/9708310.

[8] V. Barger, M.S. Berger, J.F. Gunion and T. Han, *Phys. Rev.* **D55** (1997) 142;
T. Han, Fermilab-Conf-97/080-T, hep-ph/9704215.

[9] I. Kuss and H. Spiesberger, *Phys. Rev.* **D53** (1996) 6078.

[10] J.M. Cornwall, D.N. Levin and G. Tiktopoulos, *Phys. Rev.* **D10** (1974) 1145;
G.J. Gounaris, R. Kögerler and H. Neufeld, *Phys. Rev.* **D34** (1986) 3257;
M.S. Chanowitz and M.K. Gaillard, *Nucl. Phys.* **B261** (1985) 379.

[11] A. Denner, S. Dittmaier and R. Schuster, *Nucl. Phys.* **B452** (1995) 80.

[12] G. Jikia, *Nucl. Phys.* **B494** (1997) 19.

[13] A. Denner, S. Dittmaier and T. Hahn, *Phys. Rev.* **D56** (1997) 117.

[14] The LEP collaborations ALEPH, DELPHI, L3, OPAL, the LEP Electroweak Working Group and the SLD Heavy Flavor Group (D. Abbaneo et al.), CERN-PPE/96-183;
D. Ward, talk given at the International Europhysics Conference on High-Energy Physics, Jerusalem, August 19–26, 1997.

[15] D.A. Ross and J.C. Taylor, *Nucl. Phys.* **B51** (1973) 125, E:*Nucl. Phys.* **B58** (1973) 643;
A. Sirlin, *Phys. Rev.* **D22** (1980) 971;
K. I. Aoki et al., *Suppl. Prog. Theor. Phys.* **73** (1982) 1;
M. Böhm, W. Hollik and H. Spiesberger, *Fortschr. Phys.* **34** (1986) 687.

[16] A. Denner, *Fortschr. Phys.* **41** (1993) 307.

[17] A. Denner, S. Dittmaier and G. Weiglein, *Nucl. Phys.* **B440** (1995) 95.

[18] A. Denner and S. Dittmaier, *Phys. Rev.* **D54** (1996) 4499.

[19] J. Küblbeck, M. Böhm and A. Denner, *Comp. Phys. Commun.* **60** (1991) 165;
H. Eck and J. Küblbeck, *Guide to FeynArts 1.0*, Universität Würzburg (1992);
H. Eck, *FeynArts 2.0—A generic Feynman diagram generator*, Dissertation, Universität Würzburg (1995).

[20] J.A.M. Vermaseren, *Symbolic Manipulation with FORM*, CAN, Amsterdam (1991).

[21] G.J. van Oldenborgh and J.A.M. Vermaseren, *Z. Phys.* **C46** (1990) 425.

[22] G. 't Hooft and M. Veltman, *Nucl. Phys.* **B153** (1979) 365.

[23] W. Beenakker et al., *Nucl. Phys.* **B410** (1993) 245 and *Phys. Lett.* **B317** (1993) 622.

[24] O. Cheyette and M.K. Gaillard, *Phys. Lett.* **B197** (1987) 205;
O. Cheyette, *Nucl. Phys.* **B297** (1988) 183.

[25] K. Riesselmann, *Phys. Rev.* **D53** (1996) 6226.

[26] S. Dittmaier and C. Grosse-Knetter, *Nucl. Phys.* **B459** (1996) 497.

[27] R. Mertig, M. Böhm and A. Denner, *Comp. Phys. Commun.* **64** (1991) 345;
R. Mertig, *Guide to FeynCalc 1.0*, Universität Würzburg (1992).

[28] Particle Data Group (P.M. Barnett et al.), *Phys. Rev.* **D54** (1996) 1;
J.L. Rosner, EFI-97-18, hep-ph/9704331.

[29] S. Eidelman and F. Jegerlehner, *Z. Phys.* **C67** (1995) 585;
H. Burkhardt and B. Pietrzyk, *Phys. Lett.* **B356** (1995) 398.

[30] Y.-P. Yao and C.-P. Yuan, *Phys. Rev.* **D38** (1988) 2237;
J. Bagger and C. Schmidt, *Phys. Rev.* **D41** (1990) 264;
H.-J. He, Y.-P. Kuang and X. Li, *Phys. Rev. Lett.* **69** (1992) 2619 and *Phys. Rev.* **D49** (1994) 4842.

[31] H.P. Stapp, *Nuovo Cimento* **32** (1964) 103;
J. Gunson, *J. Math. Phys.* **6** (1965) 827, 845, 852;
R.G. Stuart, *Phys. Rev. Lett.* **70** (1993) 3193.